Chiral spin liquid in a $\mathbb{Z}_3$ Kitaev model

Li-Mei Chen,[1,2] Tyler D. Ellison,[3] Meng Cheng,[3,*] Peng Ye,[1,2,†] and Ji-Yao Chen[1,4,‡]

[1]*Guangdong Provincial Key Laboratory of Magnetoelectric Physics and Devices, School of Physics, Sun Yat-sen University, Guangzhou 510275, China*

[2]*State Key Laboratory of Optoelectronic Materials and Technologies, Sun Yat-sen University, Guangzhou 510275, China*

[3]*Department of Physics, Yale University, New Haven, Connecticut 06511-8499, USA*

[4]*Center for Neutron Science and Technology, Sun Yat-sen University, Guangzhou 510275, China*

(Received 26 February 2023; revised 22 February 2024; accepted 10 April 2024; published 25 April 2024)

We study a $\mathbb{Z}_3$ Kitaev model on the honeycomb lattice with nearest neighbor interactions. Based on matrix product state simulations and symmetry considerations, we find evidence that, with ferromagnetic isotropic couplings, the model realizes a chiral spin liquid, characterized by a possible $U(1)_{12}$ chiral topological order. This is supported by simulations on both cylinder and strip geometries. On infinitely long cylinders with various widths, scaling analysis of entanglement entropy and maximal correlation length suggests that the model has a gapped two-dimensional bulk. The topological entanglement entropy is extracted and found to be in agreement with the $U(1)_{12}$ topological order. On infinitely long strips with moderate widths, we find the model is critical with a central charge consistent with the chiral edge theory of the $U(1)_{12}$ topological phase. We conclude by discussing several open questions.

DOI: 10.1103/PhysRevB.109.155161

I. INTRODUCTION

Quantum spin liquids are highly entangled phases of matter, characterized by fractionalized excitations and emergent gauge fields [1–3]. The physics of spin liquids is exemplified by the Kitaev honeycomb model, which is a remarkable example of an exactly solvable model that exhibits both gapped and gapless spin liquid phases [4]. Furthermore, when the interactions are isotropic and the time-reversal symmetry is broken (by either a small magnetic field or a three-spin interaction), the model is in a chiral spin liquid (CSL) phase, characterized by the Ising topological order. The CSL phase supports non-Abelian Ising anyons in the bulk, which can be utilized for topological quantum information processing [5]. Via the bulk-boundary correspondence, it also has gapless edge states described by a chiral Ising conformal field theory (CFT) [4], which can provide the smoking-gun evidence for experimental realizations of the Kitaev model through thermal Hall measurements [6].

Besides rapid progress towards realizing the Kitaev model experimentally [7–11], generalizations of this model, including relevant non-Kitaev-type interactions [12,13], higher spins [14,15], and various lattices [16,17], have also been under intensive investigation. These generalizations share the common property that the fractionalized degrees of freedom contain fermions. One notable exception is the generalized Kitaev model on spin-1 degrees of freedom proposed in Ref. [18], which we shall call the $\mathbb{Z}_3$ Kitaev model hereafter. In the $\mathbb{Z}_3$ Kitaev model, the local spin degrees of freedom fractionalize into $\mathbb{Z}_3$ parafermions. Using a coupled-wire construction, Ref. [18] suggested that the $\mathbb{Z}_3$ Kitaev model could support a $\mathbb{Z}_3$ parafermion topological order.

However, in contrast to the original Kitaev model, which can be solved exactly using a Majorana fermion representation [4,19], the $\mathbb{Z}_3$ Kitaev model is not exactly solvable. This is due to the fact that the Hamiltonian terms are quadratic in the $\mathbb{Z}_3$ parafermion operators, implying that the system is interacting as opposed being a free theory. Although it has been shown that a $\mathbb{Z}_3$ toric code topological phase exists in the highly anisotropic parameter region of the $\mathbb{Z}_3$ Kitaev model, much less is known about the case of isotropic couplings, which could provide a fertile ground for exotic spin liquids.

Remarkably, despite the $\mathbb{Z}_3$ Kitaev model not being exactly solvable, it possesses certain generalized symmetries that enforce the existence of a set of anyonic excitations under the assumption of a spectral gap. These symmetries are sufficient for predicting only a subset of the anyons present in the theory. Thus, more systematic work is needed to clarify the nature of the phase at the isotropic point.

In this work, we study the $\mathbb{Z}_3$ Kitaev model numerically using matrix product states to complement the symmetry considerations. Based on results on cylinder and strip geometries, we found evidence that the model at the ferromagnetic isotropic point is gapped and realizes a chiral spin liquid phase. Our numerically measured topological entanglement entropy and chiral central charge suggest an exotic $U(1)_{12}$ chiral topological order in this phase, in contrast to the $\mathbb{Z}_3$ parafermion topological order suggested in Ref. [18].

II. $\mathbb{Z}_3$ KITAEV MODEL AND SYMMETRIES

The $\mathbb{Z}_3$ Kitaev model of Ref. [18] is defined on a hexagonal lattice with a three-dimensional Hilbert space at each vertex.

*m.cheng@yale.edu
†yepeng5@mail.sysu.edu.cn
‡chenjiy3@mail.sysu.edu.cn

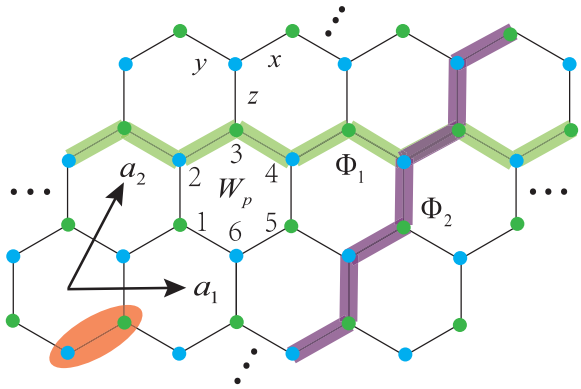

FIG. 1. Honeycomb lattice for the $\mathbb{Z}_3$ Kitaev model, generated by translations along the $\mathbf{a}_1 = (1, 0)^{\mathrm{T}}$ and $\mathbf{a}_2 = (\frac{1}{2}, \frac{\sqrt{3}}{2})^{\mathrm{T}}$ directions with a two-site unit cell. The A (B) sublattice is shown by green (blue) dots. Three different classes of links are labeled by x, y, and z. The length of the system in the $\mathbf{a}_1$ ($\mathbf{a}_2$) direction is denoted as L_x (L_y). Conserved quantities W_p, Φ_1, and Φ_2 are indicated.

We label the links of the lattice by $\alpha = x, y, z$, according to Fig. 1. The Hamiltonian is given by

$$H = -\sum_{\alpha=x,y,z} J_\alpha \sum_{\langle ij\rangle\in\alpha\text{-links}} T_i^\alpha T_j^\alpha + \mathrm{H.c.} \tag{1}$$

Here, T_i^x, T_i^y, and T_i^z are unitary operators supported at vertex i, defined by the following relations: $(T_i^x)^3 = (T_i^y)^3 = (T_i^z)^3 = 1$, $T_i^z \equiv (T_i^x T_i^y)^\dagger$, and $T_i^x T_i^y = \omega T_i^y T_i^x$, where $\omega \equiv e^{\frac{2\pi i}{3}}$. Explicit expressions of $T^{x,y,z}$ are given in Appendix A. Note that the Hamiltonian in Eq. (1) is complex instead of being real, suggesting the time reversal symmetry is broken. This is in stark contrast to the original Kitaev model.

Similar to the original Kitaev model, the Hamiltonian in Eq. (1) has an extensive number of conserved quantities. For each hexagon p, the conserved quantity W_p is defined as $W_p = (\omega T_1^x T_2^y T_3^z T_4^x T_5^y T_6^z)^\dagger$, where the operators are labeled by the vertices of p, as shown in Fig. 1. It can be checked that these W_p's are mutually commuting. More generally, for any contractible path γ, one can define a closed string operator along γ by multiplying the W_p's over the plaquettes in the region enclosed by γ.

The $\mathbb{Z}_3$ Kitaev model also has conserved quantities supported along noncontractible paths. For example, the string operator Φ_1, supported along path γ_1 in the $\mathbf{a}_1$ direction (Fig. 1), is defined as $\Phi_1 = \prod_{i\in\gamma_1}(T_i^z)^{s_i}$, where $s_i = 1(-1)$ for the $i \in A(B)$ sublattice. Similarly, the string operator Φ_2 is given by $\Phi_2 = \prod_{i\in\gamma_2}(T_i^y)^{s_i}$, where γ_2 is the path along the $\mathbf{a}_2$ direction. These conserved quantities satisfy the relation $\Phi_1\Phi_2 = \omega\Phi_2\Phi_1$, implying that every energy level of the Hamiltonian has a threefold degeneracy. We note that the set of conserved quantities generated by W_p, Φ_1, and Φ_2 form a generalized $\mathbb{Z}_3$ symmetry, known as a $\mathbb{Z}_3$ one-form symmetry [20]. See Refs. [21–23] for more details.

The conserved quantities described above in fact imply that every gapped phase captured by the Hamiltonian in Eq. (1) must host anyons of the so-called $\mathbb{Z}_3^{(2)}$ anyon theory [23,24]. To make this explicit, we consider truncations of the conserved string operators. If the string operator is truncated to an open path γ, then the truncated string operator $W(\gamma)$ fails to commute with H only at the two end points of γ. This suggests that, if the system is in a gapped phase, the open string operator $W(\gamma)$ creates anyonic excitations at its end points (see Ref. [23] for a more precise statement). Motivated by this, we can assign an Abelian anyon theory to the algebra of string operators. The properties of the associated anyons (i.e., fusion rules, exchange statistics, and braiding) are entirely determined by the algebra of string operators.

In particular, since the closed string operators satisfy the relation $W(\gamma)^3 = 1$, the anyons obey $\mathbb{Z}_3$ fusion rules. The exchange statistics θ can be computed from segments of string operators using the methods of Refs. [25,26]. We find that the anyons created by the open string operator $W(\gamma)$ have exchange statistics $\theta = e^{\frac{4\pi i}{3}}$. The $\mathbb{Z}_3$ fusion rules and $\theta = e^{\frac{4\pi i}{3}}$ exchange statistics uniquely determine that the Abelian anyon theory is $\mathbb{Z}_3^{(2)}$. The total quantum dimension of the $\mathbb{Z}_3^{(2)}$ anyon theory is $\mathcal{D} = \sqrt{3}$, and the chiral central charge is $c_- = -2 \bmod 8$.

In general, the anyon theories of the gapped phases of the $\mathbb{Z}_3$ Kitaev model factorize as $\mathcal{C} \boxtimes \mathbb{Z}_3^{(2)}$, where $\boxtimes$ denotes that anyon theories $\mathcal{C}$ and $\mathbb{Z}_3^{(2)}$ are independent [27]. The total quantum dimension of the product anyon theory $\mathcal{C} \boxtimes \mathbb{Z}_3^{(2)}$ factorizes as $\mathcal{D} = \mathcal{D}_\mathcal{C}\sqrt{3}$, where $\mathcal{D}_\mathcal{C}$ is the total quantum dimension of $\mathcal{C}$. The chiral central charges are additive, so the total chiral central charge is $c_- = c'_- - 2 \bmod 8$, with c'_- being the chiral central charge of $\mathcal{C}$.

As a concrete example, in the anisotropic limit $J_z \gg J_x, J_y$, the model can be mapped to a $\mathbb{Z}_3$ toric code [18], which corresponds to $\mathcal{C} = \mathbb{Z}_3^{(1)}$. In this case, $\mathcal{D}_\mathcal{C} = \sqrt{3}$, and $c'_- = 2 \bmod 8$. Therefore, the total quantum dimension of $\mathbb{Z}_3^{(1)} \boxtimes \mathbb{Z}_3^{(2)}$ is $\mathcal{D} = 3$, and the total chiral central charge is $c_- = 0 \bmod 8$.

The Hamiltonian also has a global $\mathbb{Z}_3$ symmetry, generated by $U = \prod_{i\in A} T_i^z \prod_{j\in B}(T_j^z)^\dagger$, with A and B denoting the two sublattices. The symmetry U can be naturally understood in terms of the $\mathbb{Z}_3$ one-form symmetry, as it is the product of Φ_1 operators over all of the paths along the $\mathbf{a}_1$ direction.

Before presenting the numerical results, we comment on the interplay between the conserved quantities and the global symmetries of the system on a cylindrical geometry. In particular, we consider a cylinder that is periodic in the $\mathbf{a}_2$ direction and has a circumference of $L_y \neq 0 \bmod 3$. We also assume, in agreement with the numerical results below, that the ground states are eigenstates of the W_p's with an eigenvalue of $W_p = \omega^n$, where $n \neq 0 \bmod 3$. From this, we draw the following two conclusions: (1) the global $\mathbb{Z}_3$ symmetry is spontaneously broken, so if the symmetry is enforced on the ground state, then it will be a Schrödinger's cat state, and (2) if the symmetry is not enforced and we consider a ground state that breaks the symmetry, then the translation symmetry in the $\mathbf{a}_1$ direction must also be broken.

To see conclusion 1, we first note that, since $L_y \neq 0 \bmod 3$, the string operator Φ_2, which wraps around the cylinder, is charged under the global $\mathbb{Z}_3$ symmetry. To show that the $\mathbb{Z}_3$ symmetry is spontaneously broken, it is sufficient to show that Φ_2 has long-range correlations. Letting $\Phi_{2,x}$ be the string operator Φ_2 supported on sites sharing the same coordinate of the $\mathbf{a}_1$ axis (denoted as x), we compute the correlator

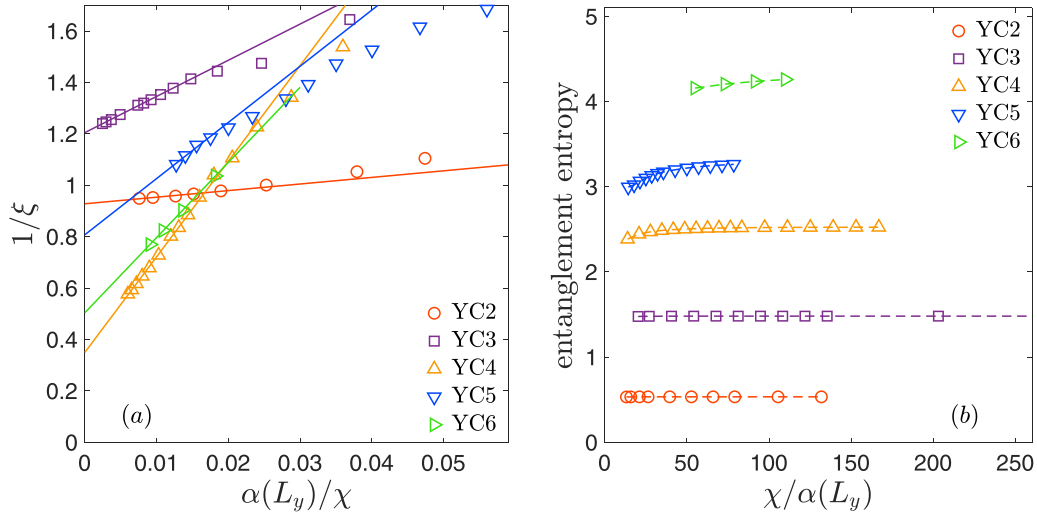

FIG. 2. Correlation length and half-cylinder entanglement entropy for infinitely long cylinders with YCL_y geometries and L_y between 2 and 6. To compare results for all computed cylinders, we have rescaled the bond dimension χ by $\alpha(L_y) = \exp(L_y/1.5)$. In (a), solid lines are a linear fit using the last few points with large χ. We note that the y intercept is nonzero, implying that for large bond dimensions, the correlation length saturates to a finite value. In (b), dashed lines are a guide to the eyes.

$\langle \Phi_{2,x}\Phi^\dagger_{2x'}\rangle$. This is nonvanishing in the limit of a large separation between x and x' because $\Phi_{2,x}\Phi^\dagger_{2x'}$ is equivalent to a product of W_p operators over the region between x and x'. Thus, using the fact that the ground states are eigenstates of the W_p's, we have $\langle \Phi_{2,x}\Phi^\dagger_{2x'}\rangle = \omega^{n|x-x'|L_y}$. A consequence is that, if the global $\mathbb{Z}_3$ symmetry is enforced, the system is in a Schrödinger's cat state.

To see conclusion 2, we notice that $\langle \Phi_{2,x}\rangle = \langle \Phi_{2,x}\Phi^\dagger_{2,x+1}\Phi_{2,x+1}\rangle$. Since $\Phi_{2,x}\Phi^\dagger_{2,x+1}$ is equivalent to a product of W_p's in the column between x and $x+1$, we have $\langle \Phi_{2,x}\rangle = \omega^{nL_y}\langle \Phi_{2,x+1}\rangle$. This implies that, if the global $\mathbb{Z}_3$ symmetry is not enforced and $\langle \Phi_{2,x}\rangle \neq 0$, then the translation symmetry in the $\mathbf{a}_1$ direction is spontaneously broken.

III. RESULTS ON CYLINDER GEOMETRY

Let us start with the cylinder geometry, i.e., periodic boundary condition along the $\mathbf{a}_2$ direction and varying circumference L_y. Following Ref. [28], we denote this class of clusters as YCL_y. Hereafter, we focus on the parameters $J_x = J_y = J_z = 1$ and use the matrix product state (MPS) based infinite density matrix renormalization group (iDMRG) algorithm to probe bulk properties [29–32]. The main physical observables to consider include the maximal correlation length ξ (extracted from the transfer matrix of the MPS) and entanglement entropy $S = -\mathrm{tr}(\rho_A \ln \rho_A)$, where ρ_A is the reduced density matrix for the left half of infinitely long cylinders. The results are shown in Fig. 2.

For a gapped system, we expect that the maximal correlation length ξ and entanglement entropy S for a width-L_y cylinder saturate to a finite value in the infinite bond dimension limit. This is clearly observed for YC2 and YC3 cylinders, as shown in Fig. 2. In these two cases, the truncation errors with the largest bond dimensions considered ($\chi_{\max} =$ 500, 3000 for YC2, YC3, respectively) are less than 10^{-10}, in agreement with the rapid saturation behavior. For YC4, 5, 6 geometry, since the required MPS bond dimension χ for a given accuracy grows exponentially with L_y, it becomes challenging to achieve full saturation of ξ. Nevertheless, the entanglement entropy clearly saturates with increasing χ, and the truncation error is around 3×10^{-7} (3×10^{-5}, 6×10^{-5}), with $\chi_{\max} = 2400(2200, 6000)$ for YC4(5, 6), respectively. A linear in $1/\chi$ fit indicates that the true correlation length in the infinite-χ limit is less than 3 lattice spacing, which indeed agrees with the existence of a spectral gap in these geometries.

Some remarks are in order. First, for all the data shown in Fig. 2, the ground states are simultaneous eigenstates of W_p and Φ_2. And on all considered cylinders, the ground state has a uniform $\mathbb{Z}_3$ flux with $\langle W_p\rangle = \omega^2$ on each plaquette, in contrast to the flux-free ground state in the original Kitaev model [4]. This was further confirmed on a small torus using exact diagonalization and on finite cylinders ($L_y = 3, L_x = 6$, 12 and $L_y = 4, L_x = 12$) using the density matrix renormalization group (DMRG). As mentioned above, the nontrival flux means that the unit cell of the MPS in iDMRG simulation is at least three columns for $L_y \neq 0$ mod 3. For YC3 and YC6 geometries, we have checked that MPS ansatzes with unit cells of one column and three columns give the same result.

Second, as discussed above, when L_y is not a multiple of 3, if the $\mathbb{Z}_3$ symmetry is imposed on the MPS, the ground state found using the iDMRG is a Schrödinger cat state with diverging correlation length. Thus, we do not impose the $\mathbb{Z}_3$ symmetry for YC2, 4, 5 cylinders. For YC3, 6, we have checked that the results obtained using $\mathbb{Z}_3$ symmetry with total charge $Q = 0$ are identical to those without using this good quantum number for relatively small bond dimensions [33]. This allows us to use the $\mathbb{Z}_3$ symmetry for YC3, 6 to reach a larger bond dimension. The $\mathbb{Z}_3$ symmetry operator in Eq. (1) is not uniform on every site, and one can apply a charge conjugation transformation on one sublattice to make it easy to exploit for MPS calculations; see Appendix A for further details about the transformation.

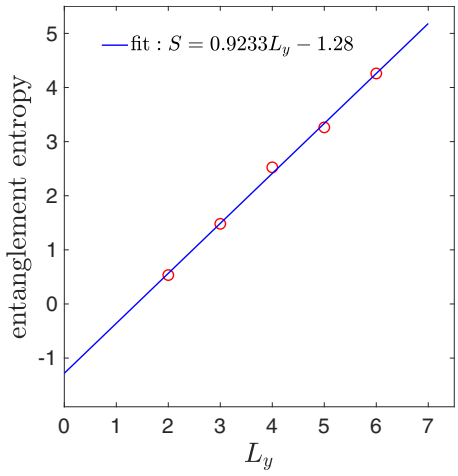

FIG. 3. Entanglement entropy versus L_y on infinitely long cylinders. For each L_y, we take the value with the largest χ. A linear fit reveals a finite TEE $S_{\text{top}} = 1.28 \pm 0.34$.

While it is difficult to make definite conclusions, our results are consistent with a gapped state in the two-dimensional (2D) bulk. If this is indeed the case, then the bulk must be topologically ordered due to the $\mathbb{Z}_3$ one-form symmetry. In the following we study possible signatures of the topological order.

A defining feature of intrinsic topological order is long-range entanglement in the ground state [34,35]. Given any region A in a gapped state, the entanglement entropy generally takes the form $S_A = \text{const} \times |\partial A| - S_{\text{top}} + \cdots$, where $|\partial A|$ denotes the length of the boundary of A, S_{top} is a universal constant known as the topological entanglement entropy (TEE), and $\cdots$ includes terms vanishing for large A. For a planar system, $S_{\text{top}} = \ln \mathcal{D}$, where $\mathcal{D}$ is the total quantum dimension of the underlying topological order. If we choose the entanglement cut along the cylinder circumference [36], S_{top} depends on which ground state the system is in. If the ground state has a definite anyon flux a through the cylinder [equivalently, as a quasi-one-dimensional system the state is short-range correlated], then $S_{\text{top}} = \ln \frac{\mathcal{D}}{d_a}$, with d_a being the quantum dimension of anyon type a. (Note that for Abelian anyon theories, such as $\mathbb{Z}_3^{(2)}$, we can take $d_a = 1$ for all a.)

In Fig. 3, we show the entanglement entropy versus cylinder width L_y (for L_y between 2 and 6), from which a nonzero TEE $S_{\text{top}} = 1.28 \pm 0.34$ is extracted. Assuming that the ground states are in the identity sector of the topological order [37], we have $S_{\text{top}} = \ln \mathcal{D}$, which gives $\mathcal{D} \approx 3.6$.

Besides entanglement entropy, chiral topological order could also be revealed by the entanglement spectrum (ES) of bipartitioning the cylinder into two halves [38]. Indeed, the Li-Haldane conjecture states that the low-energy content of the ES is described by the CFT governing the physical edge properties, which has also been extensively used in characterizing the chiral topological phase [39,40]. Here, the conserved quantities W_p lead to extensive degeneracy in the ES [41,42], making it hard to identify further structures numerically (such as the chiral CFT tower). Some examples of ES are shown in Appendix B. Nevertheless, we can probe edge properties by studying the system on a strip geometry.

IV. RESULTS ON STRIP GEOMETRY

The above study on a cylindrical geometry reveals bulk properties of the $\mathbb{Z}_3$ Kitaev model, such as the existence of a spectral gap and the total quantum dimension. Using the bulk-edge correspondence, the edge theory of this model would be given by a $1+1$D chiral CFT with central charge equal to the chiral central charge of the topological order. This can be revealed by putting the system on a strip geometry, where the chiral and antichiral gapless modes at the two edges are weakly coupled by tunneling through the bulk, with the coupling strength being exponentially suppressed by the bulk gap. Thus, for a sufficiently wide strip, one would expect to see a $1+1$D CFT (at least within a relatively large length scale), which could be tested via finite entanglement scaling.

Besides the criticality, we show in Appendix C that there is an additional 3^{L_x}-fold degeneracy on the strip geometry due to noncommuting stringlike conserved quantities that extend between the bottom and top of the strip. In the strip geometry, there are also conserved quantities $W_{p,\text{boundary}}$ corresponding to the plaquettes that would connect the top and bottom boundaries if the system were made periodic in the $\mathbf{a}_2$ direction. Numerically, we find that the expectation value of $W_{p,\text{boundary}}$ is ω or ω^2 with the same energy (exact or in the infinite-χ limit) for all the strip widths we have considered, $L_y = 2, 3, 4, 5$.

In our numerical simulations in the strip geometry, it is also important to ensure that the obtained ground states are eigenstates of Φ_2 to avoid long-range correlations from spontaneous symmetry breaking. In practice, we find that this can be achieved by starting the simulation with a small penalty term, $-\Phi_{2,x}\Phi_{2,x+1}\Phi_{2,x+2} + \text{H.c.}$ [which commutes with the Hamiltonian (1)], and the associated ground state serves as the initial state for further optimization. Alternatively, we can add $-\Phi_{2,x}$ with additional phase factor $1, \omega, \omega^2$ and its Hermitian conjugate to the Hamiltonian to enforce a specific $\langle\Phi_2\rangle$ configuration. In addition, we can also pin the conserved quantity $W_{p,\text{boundary}}$ to ω by adding a suitable pinning term.

It turns out that, for a strip of width $L_y = 2$, both the correlation length and the half-strip entanglement entropy saturate with increasing bond dimension χ, as shown in Fig. 4(a), suggesting a small finite gap. The relatively large value of the correlation length, however, indicates that the system may potentially become more critical with increasing L_y. For $L_y = 3, 4$, we observe that the system indeed becomes gapless (within the correlation length set by the bond dimension), as evidenced by the increasing correlation length and half-strip entanglement entropy with χ showing no sign of saturation. From a fit of the half-strip entanglement entropy and correlation length [43] [shown in Fig. 4(b)], we extract a central charge $c = 1.019(1.033)$ for $L_y = 3(4)$. We thus conclude that $L_y = 3$ and 4 strips have $c = 1$, which we interpret as the chiral central charge of the bulk topological order.

In addition, as a consistency check, we also performed DMRG studies on finite-size strips, where both the width and length (denoted as L_y and L_x, respectively) are finite. In this case, to fix the spectrum degeneracy, we also added Φ_2 (and

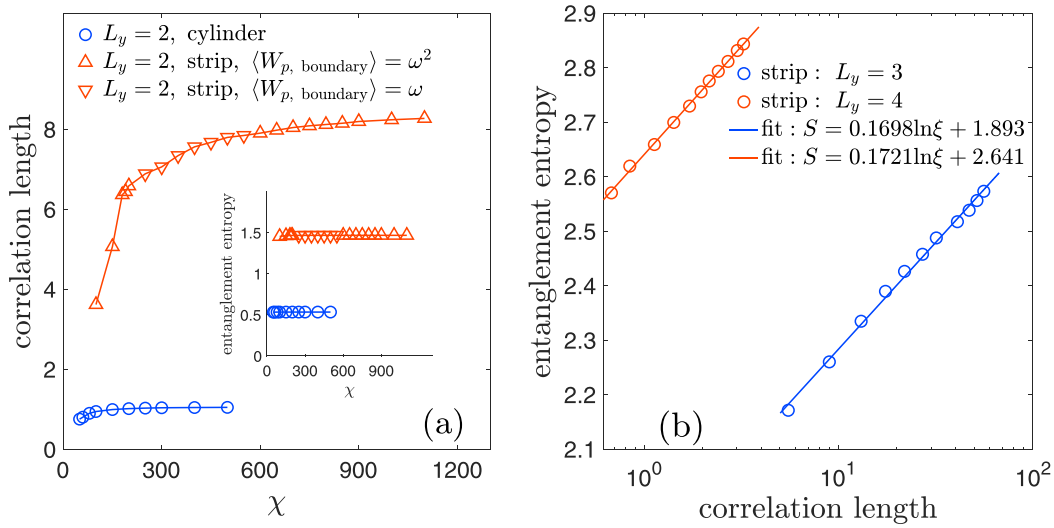

FIG. 4. (a) For the $L_y = 2$ strip, both the maximal correlation length (main panel) and entanglement entropy (inset) are converging as a function of bond dimension χ, with values significantly larger than those for the YC2 cylinder. (b) For a strip with width $L_y = 3, 4$, a diverging behavior of correlation length and entanglement entropy versus χ was found, which we fit using the finite entanglement scaling.

its Hermitian conjugate) to the Hamiltonian while taking care of the relation between Φ_2 and W_p. Typical results (among results with various bond dimensions and strip lengths) are shown in Fig. 5. It turns out that, on a sufficiently long strip with width $L_y = 2$, the entanglement entropy clearly saturates with increasing subsystem length (denoted as l), as shown in Fig. 5(a). On the contrary, on a width $L_y = 3$ strip with length $L_x = 48$, a finite central charge $c \approx 1.2$ can be extracted using the Calabrese-Cardy formula [see Fig. 5(b)] [44], which is slightly larger than the central charge on infinitely long strip possibly due to finite-size effect.

Further increasing L_y, it becomes numerically expensive to measure the central charge. Nevertheless, on $L_y = 5$ we observe that the entanglement entropy and maximal correlation length do not show any sign of saturation with increasing χ (data shown in Appendix D), consistent with the strip being gapless. Since the models are fully gapped on the cylinders, the most natural explanation of the critical properties is that they all come from the gapless edge states described by the same $c = 1$ CFT, as one would expect in a strip of a chiral topological state.

V. DISCUSSION AND CONCLUSION

In summary, we have studied the ferromagnetic isotropic point of the $\mathbb{Z}_3$ Kitaev model proposed by Barkeshli *et al.* [18]. Through a detailed study of both cylinder and strip geometries of various widths, we identified the signatures of a chiral spin liquid.

We now discuss possible topological order based on the numerical results. From the cylinder and strip calculations we have observed the following:

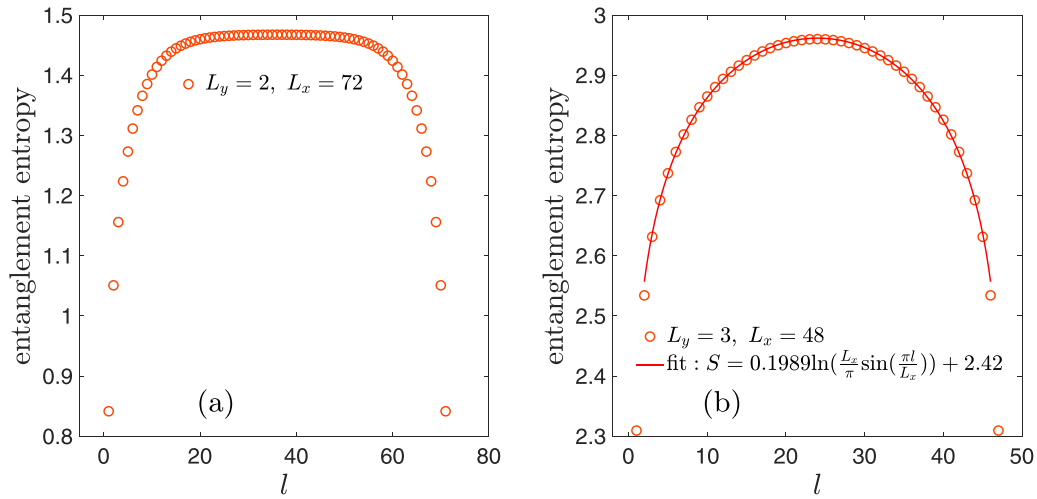

FIG. 5. Entanglement entropy of a length l subsystem on the left of a finite-size strip with total length L_x and width L_y. (a) $L_y = 2$, $L_x = 72$. The bond dimension is $\chi = 1000$, and truncation error is 5.4×10^{-11}. With increasing l, the entanglement entropy clearly saturates. (b) For $L_y = 3, L_x = 48$, the bond dimension is $\chi = 2000$, and truncation error is 4.4×10^{-7}. Using the Calabrese-Cardy formula, a central charge $c \approx 1.2$ is extracted.

(1) All cylinders up to $L_y = 6$ have finite correlation lengths, which show no sign of diverging as L_y increases.

(2) The $L_y = 3$ and 4 strips appear to be critical with $c \approx 1$.

(3) From the entanglement entropy results for cylinders we find the TEE is $S_{\text{top}} = 1.28 \pm 0.34$.

The simplest explanation of these results is that the ground state is gapped in the bulk and has gapless edge modes. Suppose the 2D topological phase has a CFT edge theory with both left- and right-moving modes and the corresponding central charges are c_L and c_R. The chiral central charge of the 2D phase is given by $c_- = c_L - c_R$, and assuming the top and bottom edges are decoupled, the strip has central charge $c = c_L + c_R$. Notice that here c_L and c_R are both non-negative. If both are positive, for a unitary CFT it is known that c_L and c_R are at least 1/2 (the Ising CFT). So we have found essentially three options:

$$(c_L, c_R) = (1, 0), (0, 1), (1/2, 1/2). \tag{2}$$

The last case means $c_- = 0$ and the edge is just a (nonchiral) Ising CFT. While this scenario cannot be excluded, we find it unlikely since there is no obvious mechanism to prevent the edge modes from opening a gap. Thus, we focus on the other two cases, where the edge modes are fully chiral.

According to the classification of chiral $c = 1$ CFTs [45], these theories come in two types: (1) $\mathrm{U}(1)_{2n}$ theories with n a nonzero integer, often referred to as the "circle branch," and (2) orbifolds of the circle branch, including $\mathbb{Z}_2$ orbifolds of $\mathrm{U}(1)_{2n}$ and three exceptional cases [orbifolding non-Abelian groups in $\mathrm{SU}(2)_1$]. We will focus on the circle branch, which turns out to be more relevant for this system. The $\mathrm{U}(1)_{2n}$ CFT can be described by a chiral compact boson. It can arise as the edge theory of a $(2+1)$-dimensional chiral topological phase, the bulk of which is described by the $\mathrm{U}(1)_{2n}$ anyon theory. An example is the $\nu = \frac{1}{2}$ bosonic Laughlin state (also known as the Kalmeyer-Laughlin state) with the $\mathrm{U}(1)_2$ chiral edge CFT. Let us enumerate the anyon content of the $\mathrm{U}(1)_{2n}$ theory. The different anyon types can be labeled by an integer defined mod $2n$, denoted as $[a]$, where $a \in \mathbb{Z}$, with $[0]$ representing the trivial excitations. $[a]$ has exchange statistics $e^{\frac{i\pi a^2}{2n}}$. The fusion rule of anyons is given by addition, so $[a] \times [b] = [a + b]$. The anyon types form a $\mathbb{Z}_{2n}$ group under fusion, with $[1]$ being the generator. Using the notations in [24], the theory is denoted as $\mathbb{Z}_{2n}^{(1/2)}$.

However, we have also established through the exact one-form symmetry of the lattice model that the bulk anyon theory must contain the $\mathbb{Z}_3^{(2)}$ as a subtheory, which places a strong constraint on the value of n. First, to have $\mathbb{Z}_3^{(2)}$ as a subtheory, $\mathbb{Z}_3$ must be a subgroup of $\mathbb{Z}_{2n}$, meaning that n must be a multiple of 3, so we write $n = 3m$. The unique $\mathbb{Z}_3$ subgroup in $\mathbb{Z}_{6m}$ is $\{[0], [2m], [4m]\}$. The self-statistics of the generator $[2m]$ is $e^{\frac{i\pi}{6m}(2m)^2} = e^{\frac{2\pi i}{3}m}$; therefore, to match $\mathbb{Z}_3^{(2)}$, m must be 2 mod 3, and n must take the form $n = 3(3k+2)$ for $k \in \mathbb{Z}$. We note that a similar analysis can exclude the orbifold branch.

To further constrain the possible values of k, we consider the TEE. It is known that the TEE for the $\mathrm{U}(1)_{6(3k+2)}$ theory is $\ln\sqrt{6|3k+2|}$. We find that compared with the fitted TEE $S_{\text{top}} = 1.28 \pm 0.34$, $k = 0$ [the $\mathrm{U}(1)_{12}$ theory] has the closet TEE, $\ln\sqrt{12} \approx 1.24$. We note that $k = -2$ [the $\mathrm{U}(1)_{-24}$ theory with TEE $\ln\sqrt{24} \approx 1.58$] is also compatible due to the relatively large error bar on the numerically computed TEE. While $\mathrm{U}(1)_{-24}$ cannot be excluded based on our data so far, we believe the fact that $\mathrm{U}(1)_{-24}$ has many more anyons and the TEE is close to the upper bound set by the error bar makes it less likely to be the actual ground state topological order. Based on this analysis, we identify $\mathrm{U}(1)_{12}$ as being the most likely candidate topological order.

Let us discuss the properties of the $\mathrm{U}(1)_{12} = \mathbb{Z}_3^{(2)} \boxtimes \mathbb{Z}_4^{(3/2)}$ anyon theory. The anyon content was discussed above. It is easy to check that [4] generates $\mathbb{Z}_3^{(2)}$ and [3] generates the $\mathbb{Z}_4^{(3/2)}$ part. This theory has 12 degenerate ground states on the torus. Starting from one of them, the others can be obtained by applying the corresponding Wilson loop operators. Since the $\mathbb{Z}_3^{(2)}$ Wilson loops commute with the Hamiltonian, the ground states (as well as all the excited states) are at least threefold degenerate. The degeneracy associated with $\mathbb{Z}_4^{(3/2)}$ is, however, not expected to be exact and is generally split by quasiparticle tunneling. Indeed, we managed to find a topologically quasidegenerate ground state on a width-3 cylinder (discussed in Appendix E). Nevertheless, due to the high topological degeneracy, finding all the topologically degenerate ground states seems to be a daunting task.

Before closing, let us also mention the open questions regarding this model. First, we should caution readers that the conclusion of a $\mathrm{U}(1)_{12}$ chiral spin liquid relies on the value of the TEE, which still shows a large error bar (see the caption of Fig. 3). Second, it is worthwhile to better understand the microscopic mechanism that can stabilize the $\mathrm{U}(1)_{12}$ topological phase in this type of model, for example, using a coupled-wire analysis. Last, currently, only the central charge is obtained from a strip geometry. It would be of great interest to extract the low-energy excitations in the same geometry, which, in principle, would allow a more complete characterization of the CFT. Given the rapid advancement of tensor network methodology [46,47], this is indeed a promising avenue to further pin down the nature of this chiral topological phase.

ACKNOWLEDGMENTS

We acknowledge conversations with J. Hauschild, X.-Y. Dong, H.-K. Jin, and H.-H. Tu. The MPS calculations were performed using the TeNPy library (version 0.9.0) [48]. L.-M.C. and P.Y. were supported by NSFC Grant No. 12074438, the Guangdong Basic and Applied Basic Research Foundation under Grant No. 2020B1515120100, and the Open Project of Guangdong Provincial Key Laboratory of Magnetoelectric Physics and Devices under Grant No. 2022B1212010008. M.C. acknowledges support from the NSF under Award No. DMR-1846109. J.-Y.C. was supported by the Open Research Fund Program of the State Key Laboratory of Low-Dimensional Quantum Physics (Project No. KF202207), the Fundamental Research Funds for the Central Universities, Sun Yat-sen University (Project No. 23qnpy60), a startup fund from Sun Yat-sen University, the Innovation Program for Quantum Science and Technology 2021ZD0302100, the Guangzhou Basic and Applied Basic Research Foundation (Grant No. 2024A04J4264), and the National Natural Science Foundation of China (NSFC) (Grant

No. 12304186). This work was also supported by the Fundamental Research Funds for Central Universities (22qntd3005). The Calculations reported were performed on resources provided by the Guangdong Provincial Key Laboratory of Magnetoelectric Physics and Devices, No. 2022B1212010008.

APPENDIX A: LOCAL OPERATORS AND CHARGE CONJUGATION

For completeness, here we first show the explicit expressions of the $T^{x,y,z}$ operators:

$$T^x = \begin{pmatrix} 0 & 0 & 1 \\ 1 & 0 & 0 \\ 0 & 1 & 0 \end{pmatrix}, \quad T^y = \begin{pmatrix} 0 & \omega^2 & 0 \\ 0 & 0 & \omega \\ 1 & 0 & 0 \end{pmatrix},$$
$$T^z = \begin{pmatrix} 1 & 0 & 0 \\ 0 & \omega & 0 \\ 0 & 0 & \omega^2 \end{pmatrix}, \tag{A1}$$

where $\omega = \exp(i2\pi/3)$.

As mentioned in the main text, the model has a global $\mathbb{Z}_3$ symmetry, generated by

$$U = \prod_{i\in A} T_i^z \prod_{j\in B} \left(T_j^z\right)^\dagger.$$

For the purpose of using symmetries to lower the computational cost, it is useful to perform a charge conjugation transformation on one of the sublattices, say, the B sublattice, to transform the generator U into a uniform form. This transformation is given by

$$\begin{aligned} CT^xC^\dagger &= (T^x)^\dagger, \\ CT^yC^\dagger &= \omega^2(T^y)^\dagger, \\ CT^zC^\dagger &= (T^z)^\dagger, \end{aligned} \tag{A2}$$

where $C = \begin{pmatrix} 1 & 0 & 0 \\ 0 & 0 & 1 \\ 0 & 1 & 0 \end{pmatrix}$.

Under this transformation, the Hamiltonian is transformed into

$$H = -\sum_{\langle ij\rangle\in x\text{-links}} J_x T_i^x \left(T_j^x\right)^\dagger - \sum_{\langle ij\rangle\in y\text{-links}} J_y\omega^2 T_i^y \left(T_j^y\right)^\dagger - \sum_{\langle ij\rangle\in z\text{-links}} J_z T_i^z \left(T_j^z\right)^\dagger + \text{H.c.},$$

and the plaquette operator W_p becomes

$$W_p = \left(T_1^x\right)^\dagger T_2^y \left(T_3^z\right)^\dagger T_4^x \left(T_5^y\right)^\dagger T_6^z.$$

The string operators Φ_1 and Φ_2 are transformed accordingly.

As noted in the main text, the $\mathbb{Z}_3$ symmetry generator commutes with the string operator Φ_2 only when L_y is a multiple of 3. Thus, one can use this $\mathbb{Z}_3$ symmetry in MPS-based calculations only for $\mathrm{mod}(L_y, 3) = 0$. For other widths with $\mathbb{Z}_3$ symmetry exploited, a Schrödinger cat state is typically observed.

APPENDIX B: ENTANGLEMENT SPECTRUM ON CYLINDERS

It is known that for chiral topological phases, the entanglement spectrum (ES) provides a valuable diagnosis [38] which is also accessible from the MPS. However, as shown in Fig. 6, the ES for the $\mathbb{Z}_3$ Kitaev model on infinitely long cylinders is heavily degenerate, with no sign of conformal towers. As noted by Ref. [42] in the context of the original Kitaev model, the degeneracy in the ES can be understood from the conserved quantities W_p. Since the logic basically follows from Ref. [42], we will not elaborate on the derivation of the degeneracy in ES and refer to Ref. [42] for further details.

APPENDIX C: DEGENERACY ON THE STRIP GEOMETRY

Here, we argue that there is at least a 3^{L_x}-fold degeneracy of the $\mathbb{Z}_3$ Kitaev model on a striplike geometry with length L_x in the $\mathbf{a}_1$ direction and width L_y in the $\mathbf{a}_2$ direction. To see

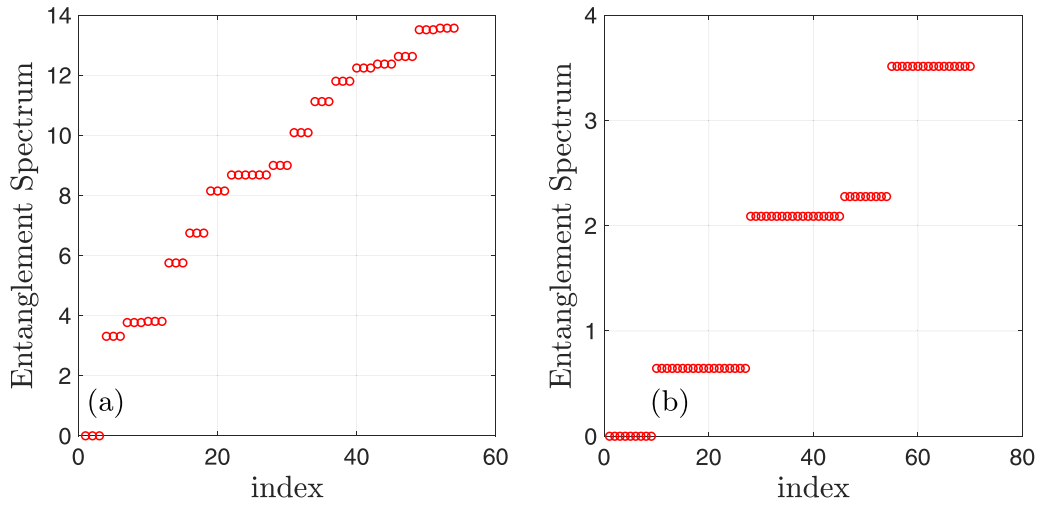

FIG. 6. Entanglement spectrum on finite-width cylinders. (a) $L_y = 3$, $\chi = 800$. (b) $L_y = 6$, $\chi = 6000$.

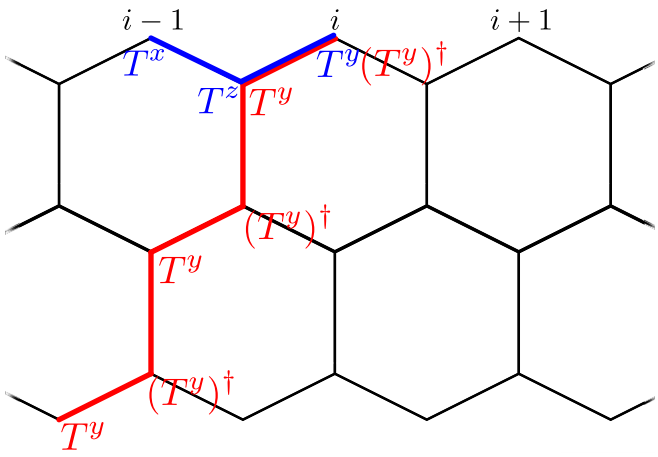

FIG. 7. The conserved quantities of the $\mathbb{Z}_3$ Kitaev model on a strip geometry are generated by the operators W_i and $\tilde{W}_i$, where i indexes the bivalent vertices at the top of the strip. The operator W_i, shown in red, is a product of T^y and $(T^y)^\dagger$ operators, while $\tilde{W}_i$, shown in blue, is a product of T^x, T^y, and T^z. If L_x is even, then each pair of W_i and $\tilde{W}_i$, for even i, generates the same operator algebra as a pair of T^x and T^y operators. This implies that each pair enforces a threefold degeneracy of the ground state. Note that $\tilde{W}_i$ and $\tilde{W}_{i-1}$ are noncommuting, so to ensure that the pairs are independent, we consider only those at even sites. The subsystem code calculation suggests that it is possible to find L_x independent noncommuting pairs.

this, we view the $\mathbb{Z}_3$ Kitaev model as a subsystem code whose gauge group is generated by products of the Hamiltonian terms. For an introduction to subsystem codes and a more careful description of the code associated with the $\mathbb{Z}_3$ Kitaev model, we refer to Ref. [23].

More specifically, we show that the subsystem code has a logical subsystem of dimension 3^{L_x}. This implies that there are L_x noncommuting pairs of conserved quantities of the $\mathbb{Z}_3$ Kitaev model that satisfy the same commutation relations as T^x and T^z. Consequently, the model must have a 3^{L_x}-fold degeneracy. To support the calculation that follows, we identify $L_x/2$ explicit pairs of noncommuting conserved quantities in Fig. 7 for a strip of even length L_x. This suffices to show that there is at least a $3^{L_x/2}$-fold degeneracy.

We now compute the dimension of the logical subsystem of the subsystem code by comparing the number of physical qutrits (i.e., three-level local degrees of freedom) to the number of stabilized qutrits and gauge qutrits. There are two qutrits for every plaquette. Due to the open boundary conditions, there are an additional $2L_x$ qutrits associated with the edges of the strip. In total, the number of qutrits $\mathbf{N}_Q$ is $\mathbf{N}_Q = 2L_xL_y$.

Next, we count the number of stabilized qutrits and the number of gauge qutrits. The only stabilizers are the conserved quantities W_p for every plaquette, each of which stabilizes a single qutrit. There are $L_x(L_y-1)$ plaquettes, so the number of stabilized qutrits $\mathbf{N}_S$ is $\mathbf{N}_S = L_x(L_y-1)$. There are three gauge generators for every plaquette. There are an additional two for every plaquette on an edge of the strip. Therefore, the number of gauge qutrits $\mathbf{N}_G$ is

$$\mathbf{N}_G = \{[3L_x(L_y-1)+2L_x] - \mathbf{N}_S\}/2 = L_xL_y. \tag{C1}$$

Here, we have subtracted $\mathbf{N}_S$ since the stabilizers are generated by the gauge generators, and we have divided by 2 to account for the fact that the operator algebra of a qutrit has two generators, T^x and T^z.

The number of logical qutrits $\mathbf{N}_L$ is then given by the formula

$$\mathbf{N}_L = \mathbf{N}_Q - \mathbf{N}_S - \mathbf{N}_G = L_x. \tag{C2}$$

Thus, there are L_x logical qutrits, which means that there are $2L_x$ generators of the logical group, each of which is a conserved quantity of the $\mathbb{Z}_3$ Kitaev model. Therefore, we conclude that there is a 3^{L_x}-fold degeneracy on a strip geometry.

We note that this degeneracy can be lifted by including a single site term in the Hamiltonian for each bivalent vertex at the boundary.

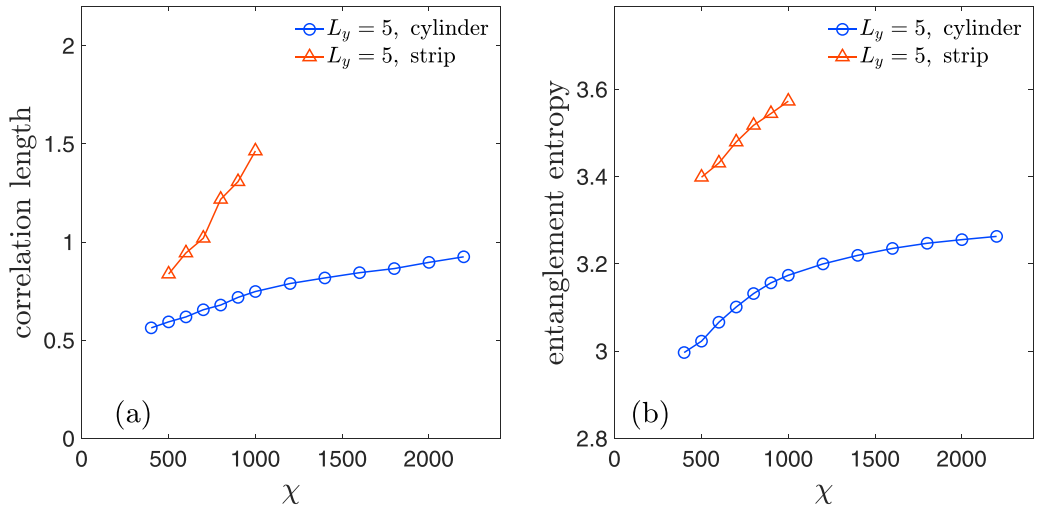

FIG. 8. Comparison of (a) the maximal correlation length and (b) entanglement entropy for an $L_y = 5$ cylinder and strip. On the strip's boundary, we have $\langle W_p \rangle = \omega$ for all data shown here.

Moreover, for the ground states on strips, under the assumption that the flux on each column is the same, which we verified numerically, we have

$$\Phi_{2,x}\Phi_{2,x+1}\Phi_{2,x+2} = \Phi_{2,x}\Phi^{\dagger}_{2,x+1}\Phi^{\dagger}_{2,x+1}\Phi_{2,x+2} = \omega^{nL_y}\cdot\omega^{-nL_y} = 1, \tag{C3}$$

where we have used the fact that product of W_p operators in one column equals $\Phi_{2,x}\Phi^{\dagger}_{2,x+1}$.

APPENDIX D: ADDITIONAL DATA FOR AN $L_y = 5$ STRIP

Here, we show additional evidence that the critical behavior can also be observed on a $L_y = 5$ strip. In Fig. 8, we compare the maximal correlation length and entanglement entropy of an $L_y = 5$ strip and cylinder. Both correlation length and entanglement entropy grow much quicker (and have larger values) on the strip geometry, without any sign of saturation. This scenario is consistent with the data for $L_y = 3, 4$ shown in the main text.

APPENDIX E: QUASIDEGENERACY ON $L_y = 3$ CYLINDER

Topological order implies (quasi)degenerate ground states on infinitely long cylinders, which can be found by running iDMRG simulations with suitable initial states [39,40]. Here, on a YC3 cylinder, by randomizing the initial state, we found that the iDMRG simulation has a nonzero probability of finding a distinct (excited) state, denoted as $|\Psi_\epsilon\rangle$, while the actual ground state is $|\Psi_1\rangle$. $|\Psi_\epsilon\rangle$ is also a simultaneous eigenstate of W_p and Φ_2, with $\langle W_p\rangle = \omega^2$. The overlap per column between $|\Psi_1\rangle$ and $|\Psi_\epsilon\rangle$ is 4.2×10^{-3}, with bond dimension $\chi = 500$, suggesting that the two states are orthogonal.

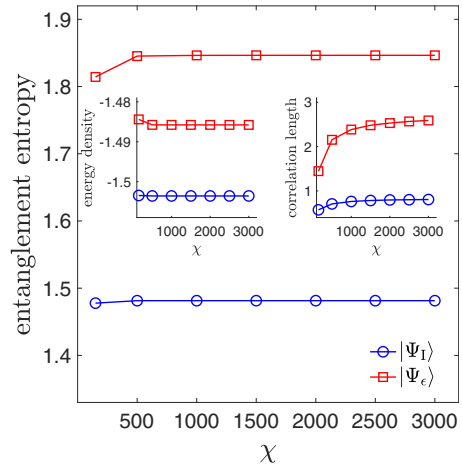

FIG. 9. Comparison of ground state properties in different topological sectors versus χ on a YC3 cylinder. Here, $|\Psi_1\rangle$ and $\Psi_\epsilon\rangle$ are ground states in distinct topological sectors. The main panel shows entanglement entropy in the two sectors, with energy density and maximal correlation length shown in the insets.

A comparison of $|\Psi_1\rangle$ and $|\Psi_\epsilon\rangle$ is shown in Fig. 9. We identify $|\Psi_\epsilon\rangle$ as an approximately degenerate ground state on the finite-circumference cylinder. Because of the finite width, the topological degeneracy will be split by virtual quasiparticle tunneling effects, which explains the energy difference shown in the left inset of Fig. 9. Moreover, on the YC3 cylinder, the maximal correlation length of $|\Psi_\epsilon\rangle$ converges with increasing bond dimension χ (shown in the right inset in Fig. 9), implying that $|\Psi_\epsilon\rangle$ is also gapped, although the value is larger than that of $|\Psi_1\rangle$. On the other hand, $|\Psi_\epsilon\rangle$ has a higher half-cylinder entanglement entropy than $|\Psi_1\rangle$, with the difference approaching 0.36 with increasing χ.

[1] G. Misguich and C. Lhuillier, Two-dimensional quantum antiferromagnets, in *Frustrated Spin Systems*, edited by H. T. Diep (World Scientific, Singapore, 2005), pp. 229–306.

[2] L. Savary and L. Balents, Quantum spin liquids: A review, Rep. Prog. Phys. **80**, 016502 (2017).

[3] Y. Zhou, K. Kanoda, and T.-K. Ng, Quantum spin liquid states, Rev. Mod. Phys. **89**, 025003 (2017).

[4] A. Kitaev, Anyons in an exactly solved model and beyond, Ann. Phys. (NY) **321**, 2 (2006).

[5] C. Nayak, S. H. Simon, A. Stern, M. Freedman, and S. Das Sarma, Non-Abelian anyons and topological quantum computation, Rev. Mod. Phys. **80**, 1083 (2008).

[6] Y. Kasahara, T. Ohnishi, Y. Mizukami, O. Tanaka, S. Ma, K. Sugii, N. Kurita, H. Tanaka, J. Nasu, Y. Motome, T. Shibauchi, and Y. Matsuda, Majorana quantization and half-integer thermal quantum Hall effect in a Kitaev spin liquid, Nature (London) **559**, 227 (2018).

[7] S. Trebst and C. Hickey, Kitaev materials, Phys. Rep. **950**, 1 (2022).

[8] H. Takagi, T. Takayama, G. Jackeli, G. Khaliullin, and S. E. Nagler, Concept and realization of Kitaev quantum spin liquids, Nat. Rev. Phys. **1**, 264 (2019).

[9] A. Micheli, G. K. Brennen, and P. Zoller, A toolbox for lattice-spin models with polar molecules, Nat. Phys. **2**, 341 (2006).

[10] K. Slagle, Y. Liu, D. Aasen, H. Pichler, R. S. K. Mong, X. Chen, M. Endres, and J. Alicea, Quantum spin liquids bootstrapped from Ising criticality in Rydberg arrays, Phys. Rev. B **106**, 115122 (2022).

[11] R. Verresen and A. Vishwanath, Unifying Kitaev magnets, kagomé dimer models, and ruby Rydberg spin liquids, Phys. Rev. X **12**, 041029 (2022).

[12] Z.-X. Liu and B. Normand, Dirac and chiral quantum spin liquids on the honeycomb lattice in a magnetic field, Phys. Rev. Lett. **120**, 187201 (2018).

[13] J. Wang, B. Normand, and Z.-X. Liu, One proximate Kitaev spin liquid in the $k-j-\Gamma$ model on the honeycomb lattice, Phys. Rev. Lett. **123**, 197201 (2019).

[14] X.-Y. Dong and D. N. Sheng, Spin-1 Kitaev-Heisenberg model on a honeycomb lattice, Phys. Rev. B **102**, 121102(R) (2020).

[15] H.-K. Jin, W. M. H. Natori, F. Pollmann, and J. Knolle, Unveiling the S=3/2 Kitaev honeycomb spin liquids, Nat. Commun. **13**, 3813 (2022).

[16] H. Yao and S. A. Kivelson, Exact chiral spin liquid with non-Abelian anyons, Phys. Rev. Lett. **99**, 247203 (2007).

[17] S. Chulliparambil, U. F. P. Seifert, M. Vojta, L. Janssen, and H.-H. Tu, Microscopic models for Kitaev's sixteenfold way of anyon theories, Phys. Rev. B **102**, 201111(R) (2020).
[18] M. Barkeshli, H.-C. Jiang, R. Thomale, and X.-L. Qi, Generalized Kitaev models and extrinsic non-Abelian twist defects, Phys. Rev. Lett. **114**, 026401 (2015).
[19] X.-Y. Feng, G.-M. Zhang, and T. Xiang, Topological characterization of quantum phase transitions in a spin-1/2 model, Phys. Rev. Lett. **98**, 087204 (2007).
[20] Here, the symmetry is distinct from the one-form symmetry introduced in Ref. [21] since the symmetry operators are not truly topological [22].
[21] D. Gaiotto, A. Kapustin, N. Seiberg, and B. Willett, Generalized global symmetries, J. High Energy Phys. 02 (2015) 172.
[22] M. Qi, L. Radzihovsky, and M. Hermele, Fracton phases via exotic higher-form symmetry-breaking, Ann. Phys. (NY) **424**, 168360 (2021).
[23] T. D. Ellison, Y.-A. Chen, A. Dua, W. Shirley, N. Tantivasadakarn, and D. J. Williamson, Pauli topological subsystem codes from Abelian anyon theories, Quantum **7**, 1137 (2023).
[24] P. H. Bonderson, Non-Abelian anyons and interferometry, Ph.D. thesis, California Institute of Technology, 2012.
[25] M. Levin and X.-G. Wen, Fermions, strings, and gauge fields in lattice spin models, Phys. Rev. B **67**, 245316 (2003).
[26] K. Kawagoe and M. Levin, Microscopic definitions of anyon data, Phys. Rev. B **101**, 115113 (2020).
[27] M. Mäger, On the structure of modular categories, Proc. London Math. Soc. **87**, 291 (2003).
[28] S. Yan, D. A. Huse, and S. R. White, Spin-liquid ground state of the S = 1/2 kagome Heisenberg antiferromagnet, Science **332**, 1173 (2011).
[29] I. P. McCulloch, Infinite size density matrix renormalization group, revisited, arXiv:0804.2509.
[30] U. Schollwöck, The density-matrix renormalization group in the age of matrix product states, Ann. Phys. (NY) **326**, 96 (2011).
[31] S. R. White, Density matrix formulation for quantum renormalization groups, Phys. Rev. Lett. **69**, 2863 (1992).
[32] E. Stoudenmire and S. R. White, Studying two-dimensional systems with the density matrix renormalization group, Annu. Rev. Condens. Matter Phys. **3**, 111 (2012).
[33] We have checked via ED that the ground state on a 12-site torus has $\mathbb{Z}_3$ charge 0.
[34] M. Levin and X.-G. Wen, Detecting topological order in a ground state wave function, Phys. Rev. Lett. **96**, 110405 (2006).
[35] A. Kitaev and J. Preskill, Topological entanglement entropy, Phys. Rev. Lett. **96**, 110404 (2006).
[36] H.-C. Jiang, Z. Wang, and L. Balents, Identifying topological order by entanglement entropy, Nat. Phys. **8**, 902 (2012).
[37] This can be justified by various random initial states giving the same result.
[38] H. Li and F. D. M. Haldane, Entanglement spectrum as a generalization of entanglement entropy: Identification of topological order in non-Abelian fractional quantum Hall effect states, Phys. Rev. Lett. **101**, 010504 (2008).
[39] L. Cincio and G. Vidal, Characterizing topological order by studying the ground states on an infinite cylinder, Phys. Rev. Lett. **110**, 067208 (2013).
[40] J.-Y. Chen, J.-W. Li, P. Nataf, S. Capponi, M. Mambrini, K. Totsuka, H.-H. Tu, A. Weichselbaum, J. von Delft, and D. Poilblanc, Abelian $\mathrm{Su}(N)_1$ chiral spin liquids on the square lattice, Phys. Rev. B **104**, 235104 (2021).
[41] H. Yao and X.-L. Qi, Entanglement entropy and entanglement spectrum of the Kitaev model, Phys. Rev. Lett. **105**, 080501 (2010).
[42] K. Shinjo, S. Sota, and T. Tohyama, Density-matrix renormalization group study of the extended Kitaev-Heisenberg model, Phys. Rev. B **91**, 054401 (2015).
[43] F. Pollmann, S. Mukerjee, A. M. Turner, and J. E. Moore, Theory of finite-entanglement scaling at one-dimensional quantum critical points, Phys. Rev. Lett. **102**, 255701 (2009).
[44] P. Calabrese and J. Cardy, Entanglement entropy and quantum field theory, J. Stat. Mech. (2004) P06002.
[45] P. H. Ginsparg, Curiosities at c = 1, Nucl. Phys. B **295**, 153 (1988).
[46] Y. Zou, A. Milsted, and G. Vidal, Conformal data and renormalization group flow in critical quantum spin chains using periodic uniform matrix product states, Phys. Rev. Lett. **121**, 230402 (2018).
[47] L. Vanderstraeten, J. Haegeman, and F. Verstraete, Tangent-space methods for uniform matrix product states, SciPost Phys. Lect. Notes 7 (2019).
[48] J. Hauschild and F. Pollmann, Efficient numerical simulations with Tensor Networks: Tensor Network Python (TeNPy), SciPost Phys. Lect. Notes 5 (2018).